https://doi.org/10.5194/egusphere-2024-250
Preprint. Discussion started: 21 February 2024

The Pléiades Glacier Observatory: high resolution digital elevation models and ortho-imagery to monitor glacier change

Etienne Berthier[1], Jérôme Lebreton[1], Delphine Fontannaz[2], Steven Hosford[2], Joaquin M. C. Belart[3], Fanny Brun[4], Liss M. Andreassen[5], Brian Menounos[6,7], Charlotte Blondel[1]

[1] Université de Toulouse, LEGOS (CNES/CNRS/IRD/UT3), Toulouse, France

[2] Centre National d'Etudes Spatiales, Toulouse, France

[3] National Land Survey of Iceland, Akranes, Iceland

[4] IGE, Université Grenoble Alpes, CNRS, IRD, Grenoble INP, Grenoble, France

[5] Section for Glaciers, Ice and Snow, the Norwegian Water Resources and Energy Directorate (NVE), Oslo, Norway

[6] University of Northern British Columbia, Prince George, BC, Canada

[7]Hakai Institute, Campbell River, BC, Canada

Correspondence to: Etienne Berthier (etienne.berthier@univ-tlse3.fr)

Abstract. Spaceborne digital elevation models (DEMs) of glaciers are essential to describe their health, and their contribution to river runoff and to sea level rise. Publicly available DEMs derived from sub-meter satellite stereo-imagery were, up to now, mainly available in the polar regions and High Mountain Asia. Here, we present the Pléiades Glacier Observatory (PGO), a scientific programme acquiring Pléiades stereo pairs for 140 sites from Earth's glacierized areas. The PGO product consists of DEMs at 2 m and 20 m ground sampling distance together with 0.5 m (panchromatic) and 2 m (multispectral) ortho-images. The DEMs are freely available to all registered users whereas ortho-images are available after signing a licence. PGO commenced in July 2016 in the North Hemisphere and February 2017 in the South Hemisphere. Each site is revisited every five years (cloud permitting), close to the end of the melt season, to measure glacier elevation change with an average uncertainty of 0.49 m (95% confidence level, for a glacierized area of 1 km²), i.e. 0.1 m a^{-1}. PGO samples over 20,000 km² of glacierized terrain which represents about 3% of the Earth's glaciers area. This small sample, however, provides a first order estimate of the global glacier mass change and its decadal evolution.

https://doi.org/10.5194/egusphere-2024-250
Preprint. Discussion started: 21 February 2024

1. Introduction

Over the last two decades, the increase in spaceborne satellite imagery archives accelerated our ability to quantify glacier change (Pope et al., 2014; Berthier et al., 2023). Distribution of medium (10-30 m) resolution satellite archives (e.g., from Landsat, ASTER) and the open nature of new missions (e.g. the Sentinels from Copernicus), for example, provided imagery to construct improved glacier inventories (Pfeffer et al., 2014; RGI 7.0 Consortium, 2023) spatiotemporal analysis of glacier velocity (Millan et al., 2022) and elevation change (Hugonnet et al., 2021). These global observational products of glacier change are important calibration data to improve projections of future glacier mass change (Rounce et al., 2023).

Glaciology has also benefited from the use of very high (i.e. sub-meter) resolution optical sensors. Contrary to medium-resolution satellite missions, present-day very high resolution satellite missions do not allow a frequent and global survey of the Earth's glaciers, but these missions are advantageous in a number of ways. The ability to quickly task these satellites provides a means for rapid response following natural disasters (Shugar et al., 2021; Kääb et al., 2021). Their sub-meter resolution translates into superior derived products (e.g. glacier outline, velocity, elevation, snow-line elevation) compared to those obtained from medium resolution imagery. This improved quality is needed to study fine scale processes (Sato et al., 2021; Brun et al., 2016; Loriaux and Ruiz, 2021), monitor small glaciers (Małecki, 2022), validate similar products derived from coarser images (Andreassen et al., 2022) and also calibrate glaciological mass balance measured in the field (Zemp et al., 2013; Wagnon et al., 2021; Andreassen et al., 2016). With the notable exceptions of the polar regions (Howat et al., 2019; Porter et al., 2018) and High Mountain Asia (Shean et al., 2020), however, access to this very high resolution data has remained limited for the glaciological community.

This article presents the Pléiades Glacier Observatory (PGO), an initiative by the French Space Agency (CNES) and the Laboratoire d'Etudes en Géophysique et Océanographie Spatiales (LEGOS) to facilitate access to very high resolution data (digital elevation models – DEMs – and ortho-imagery) from the Pléiades satellites. We present the coverage achieved since 2016 and describe how the freely-available products are derived from raw Pléiades stereo-images. We also assess the quality of the PGO DEMs using accurate lidar data acquired almost simultaneously in Norway and western Canada and evaluate the precision of the elevation change maps that are derived every five years for the 140 PGO glaciated sites. We conclude by considering how representative the geodetic mass balance derived for these PGO sites is for Earth's glaciers.

2. Design of the PGO project

2.1. Pléiades 1A and 1B satellites for glacier monitoring

CNES and Airbus Defense and Space respectively designed and operates the optical satellites Pléiades 1A and 1B (Gleyzes et al., 2012). Pléiades 1A was launched 17 December 2011 and 1B 2 December 2012. The image resolution of the panchromatic and multi-spectral bands are respectively 0.7 m and 2.8 m. In order to derive DEMs, stereo pairs or tri-stereo images can be acquired along-track about half a minute apart. Compared to earlier stereo sensors (SPOT5-HRS, ALOS-PRISM and TERRA-ASTER), a clear advantage for snow and ice monitoring is 12-bit encoding of the sensor (4096 grey levels) which

2

https://doi.org/10.5194/egusphere-2024-250
Preprint. Discussion started: 21 February 2024

significantly increases the image contrast over flat and texture-less regions, such as snow-covered areas (Berthier et al., 2023).

Early results on several glaciers showed the usefulness of Pléiades data for measuring their topography and its change with time (Berthier et al., 2014). The 1-sigma uncertainty of these Pléiades DEMs is about 1 m over gently sloping areas (Błaszczyk et al., 2019; Berthier et al., 2014). This level of uncertainty is adequate to measure elevation changes, often reaching several metres, at seasonal (Belart et al., 2017; Beraud et al., 2023) to inter-annual (Bhattacharya et al., 2021) time scales.

Airbus operates Pléiades 1A and 1B commercially which does not include building a global archive of images, at least not for glaciers. Furthermore, access to the data is difficult and cost prohibitive, especially for users outside of the European Union. These challenges led us to commence the PGO in 2016 as a way to monitor a selection of glacier sites around the globe and facilitate access for the international glaciological community.

Despite the 12-bits encoding of the images, we observed saturated pixels for early Pléiades images (2011–2015) on well illuminated slopes in the European Alps and Himalaya at the time of image acquisition (10h30 to 11h local time). No saturation was observed in the polar regions due to the lower sun incidence angles. To avoid this saturation in the tropics and mid-latitudes, a request is systematically made to Airbus DS to lower the gain within the 60°N-60°S latitude bands. Technically, it consists in requesting to lower the number of time delay integration (TDI) stages from the default value of 13 to a value of 10. Finally, we found limited added value of tri-stereo compared to a standard stereo coverage (Berthier et al., 2014), likely because most of the imaged glaciers are moderately sloped. Tri-stereo coverage being 50% more expensive for the project, PGO acquisitions are all performed in standard stereo mode.

2.2. Selected glacier targets and acquisitions campaigns

Given the funding available for the PGO, an exhaustive survey of the ~700 000 km² glaciers on Earth is not feasible. Our strategy is, instead, to focus on a discrete number of sites and propose some tailored acquisitions. In particular, we are careful to task the Pléiades satellites during a time window prescribed by experts in glacier research, in most cases at the end of the summer when the snow cover is the lowest on and off glaciers. This is important because, when snow is present, the risk of image saturation is higher and the coregistration of the DEMs is more uncertain. Late summer acquisitions also means that the images and DEMs will often be acquired close in time to the glaciological field measurements or airborne campaigns which facilitates comparisons. Reduced snow cover also means that most PGO ortho-images should be suitable to update glacier inventories (Andreassen et al., 2022; Paul et al., 2011) and to delineate the snowline, a proxy for the equilibrium line if observed close to the end of melt season (Pelto, 2010; Rabatel et al., 2013). Images in the PGO database are almost cloud free because any image with more than 10% of clouds is rejected during the tasking. If a cloud free stereo-pair is not obtained during the user-defined time period, the tasking is first extended by a few weeks (if relevant) or/and postponed to the following year.

A PGO site covers typically 100 to 500 km², and generally includes dozens of glaciers. Site selection was performed following a call to the community through the World Glacier Monitoring Service (WGMS, Zurich), the agency in charge of compiling and disseminating standardised datasets on glacier fluctuations. The reason to go through the WGMS was that Pléiades repeat DEMs have a high potential to calibrate (field) glaciological mass balance estimates (Zemp et al., 2013) and also help to assess the

3

https://doi.org/10.5194/egusphere-2024-250
Preprint. Discussion started: 21 February 2024

regional representativeness of the glaciers monitored in the field. The PGO covers several WGMS benchmark glaciers. We also included iconic glaciers (e.g., Perito Moreno in Argentina ; Kilimanjaro in Tanzania) and, as much as possible, we attempted to ensure that the PGO samples all main glacierized regions on Earth. The PGO only samples a few sites in the Arctic regions (including Alaska) because these glaciers are regularly imaged by the ArcticDEM project (Porter et al., 2018). Among the 19 GTN-G first order glacier regions (GTN-G, 2023), only the Russian Arctic is not sampled by the PGO as no request came from the research community for this region. Overall, the PGO acquires imagery over 140 targets (Figure 1, Table 1).

For funding reasons, not all sites could be observed the same year. We thus designed an acquisition program made of 10 original campaigns, five in each hemisphere. These campaigns occur during the summer and early autumn (i.e. from July to October in the north hemisphere and from January to May in the south hemisphere). During each of these campaigns, the Pléiades satellites attempted to acquire images over 10 to 30 glacier sites. The first PGO campaign took place in summer 2016 in the northern hemisphere and the last one in summer 2021 in the southern hemisphere.

Since July 2021 in the northern hemisphere (and February 2022 in the southern), the PGO has entered into repeat mode, i.e. stereo coverage is repeated five years after previous acquisitions (cloud permitting). The choice of this 5-yr time lag between acquisitions was driven by (i) the wish to have a high signal-to-noise ratio on the measurement of the rate of elevation change, and (ii) the consideration that the volume-to-mass conversion factor is not well-constrained for periods shorter than 5-years (Huss, 2013).

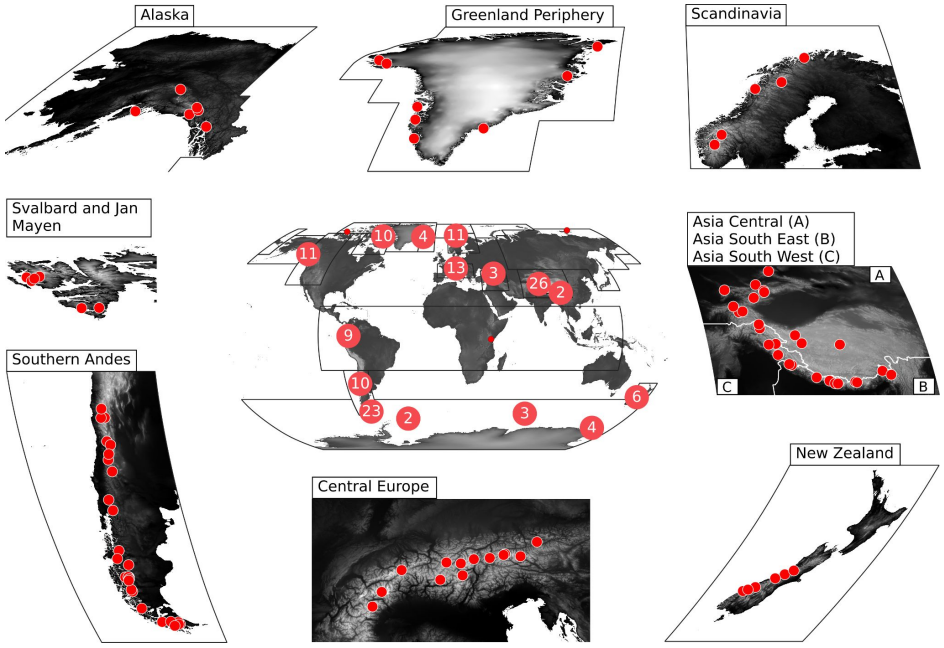

Figure 1. Map of the distribution of the 140 PGO sites. The central panel shows the number of sites in the main glacier regions and the peripheral panels highlight the distribution of the sites for a few regions of dense spatial coverage.

4

https://doi.org/10.5194/egusphere-2024-250
Preprint. Discussion started: 21 February 2024

Table 1. Summary of the areas and number of glaciers covered during the first 10 PGO original campaigns. NH stands for Northern Hemisphere, SH for Southern Hemisphere. See also Table 3 for the distribution of sites among the 19 GTN-G first order glacier regions.

Campaign	Number of sites	Total area km²	Glacier area km²	Number of glaciers*	Number of stereo pairs
2016 NH	18	7163	2514	771	30
2017 SH	14	4970	1819	813	28
2017 NH	29	11,262	4434	1469	52
2018 SH	9	3671	1535	365	22
2018 NH	13	4719	1826	573	26
2019 SH	5	3352	1911	221	23
2019 NH	14	6229	1909	1019	34
2020 SH	12	4338	1491	670	21
2020 NH	14	5276	2065	784	27
2021 SH	12	3509	1870	125	19
Total	**140**	**54,489**	**21,374**	**6810**	**282**

* Counting only glaciers for which at least 50% of the area is covered.

2.3. The PGO products

The PGO products consist of the DEMs and related ortho-images derived automatically from the stereo-pair, and the 5-year maps of elevation difference calculated once a PGO site has been observed again by the Pléiades satellite.

2.3.1. DEMs and ortho-images

Airbus Defense and Space provides Pléiades stéréo-pairs at the "primary" processing level. We then generate DEMs and ortho-images using the Ames Stereo Pipeline (ASP) (Beyer et al., 2018), version 3.0.0, release 2021-10-05 (https://github.com/NeoGeographyToolkit/StereoPipeline). ASP is a suite of free and open source tools designed for processing stereo images captured from satellites and other platforms. It is extensively used in glaciology to generate DEMs from Worldview (Shean et al., 2016; Willis et al., 2015), ASTER (Advanced Spaceborne Thermal Emission and Reflection Radiometer) on board TERRA (Brun et al., 2017; Shean et al., 2020) and Pléiades (Marti et al., 2016; Deschamps-Berger et al., 2020) satellites.

A key step for the generation of a DEM is the correlation between the two images of the stereo-pair. Several algorithms are available in ASP that can lead to different results. Deschamps-Berger et al. (2020) showed that the choice of the photogrammetric options, and in particular the correlator, has an impact on the precision and completeness of the elevation difference over stable terrain and snow-covered areas. We used their preferred set of photogrammetric options, based on the Semi-Global Matching (SGM) correlator (Hirschmuller, 2008). SGM has the advantage of providing a highly-resolved topography and a limited amount of data gaps. However, we observed that in some cases (Figure 2), SGM tended to fill the DEM with noisy data in textureless areas of the images (cast shadows, areas covered with fresh snow, saturated images). For this reason, we also processed the stereo-pairs using the block-matching (BM) correlator with a set of processing parameters taken from (Willis et al., 2015; Marti et al., 2016). We provide both versions (SGM and BM) and leave it to the user with their local knowledge of the study

5

https://doi.org/10.5194/egusphere-2024-250
Preprint. Discussion started: 21 February 2024

area to decide which version of the DEM (or a combination of both) is the most appropriate for a given study. We produced 2 and 20 m DEMs from the native point clouds generated by ASP. The 20-m DEM is a smoother version that can be useful for testing some methodologies on smaller files and for generating more complete ortho-images as it contains less data gaps.

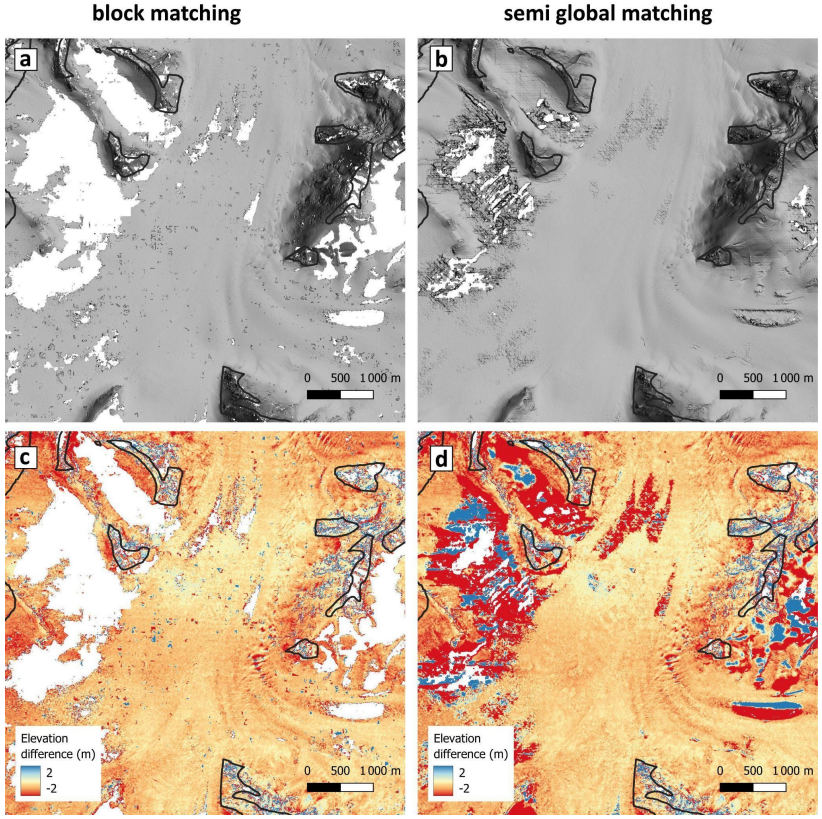

Figure 2. Comparison of the Pléiades 2-m DEMs derived using the BM (left) and SGM (right) algorithms of the Ames Stereo Pipeline (ASP) for the upper accumulation area of Fedchenko glacier (Pamir, Central Asia). Upper panels a and b show shaded relief images of the 2019-08-01 DEMs. Lower panels c and d show the elevation differences between these 2019-08-01 and the 2019-09-22 Pléiades DEMs. Note that the locations where data gaps are present in the BM DEMs (white areas in panels a and c) correspond to unrealistically high/low values in the SGM elevation difference map (panel d).

In our workflow, 0.5 m panchromatic and 2 m multispectral ortho-images are generated using the 20-m DEM. Pansharpened images (i.e. multispectral images at 0.5 m resolution) are not calculated and archived due to file storage limitations. These pansharpened images, however, could easily be generated by the user using freely available tools such as *pansharp* in ASP or *otbcli_Pansharpening* in the Orfeo ToolBox (https://www.orfeo-toolbox.org/).

Native geolocation performance is 8.5 m (CE90, Circular Error at a confidence level of 90 %) for Pléiades-1A and 4.5 m for Pléiades-1B (Lebègue et al., 2015) without ground control points (GCPs). Further, Pléiades DEMs derived without GCPs can be biased in height by as much as 10 to 20 m. To avoid such large horizontal and vertical shifts and to ensure an improved consistency of the PGO database, all DEMs

6

https://doi.org/10.5194/egusphere-2024-250
Preprint. Discussion started: 21 February 2024

are coregistered to the Copernicus GLO-30 DEM (GLO-30) using the implementation by Shean et al. (2016) (https://github.com/dshean/demcoreg) of the Nuth and Kääb (2011)'s algorithm. GLO-30, an edited version of the TanDEM-X DEM, was chosen as a reference DEM because it is currently the best global void free DEM publicly available (Franks and Rengarajan, 2023). Given the time lag between the radar images used to produce the TanDEM-X DEM (2011 to 2015, (Rizzoli et al., 2017)) and the PGO acquisitions, coregistration was performed on stable terrain, masking out glaciers as inventoried in the RGI v6.0 (RGI Consortium, 2017). For a few test sites, we found that the coregistration vectors were almost unchanged when using the 20 m instead of the 2 m DEM. Hence, the shift vectors were computed using the 20 m DEMs (a ground sampling distance closer to the one of GLO-30) and the shifts were applied to all PGO products (2-m and 20-m DEMs and all ortho-images).

Figure 3 shows one of the PGO products (DEM and ortho-images) and the elevation difference to GLO-30 before and after coregistration for a portion of the Purogangri ice cap over the Tibetan Plateau. An example of the fact sheet that accompanies each PGO product is available in Appendix A1.

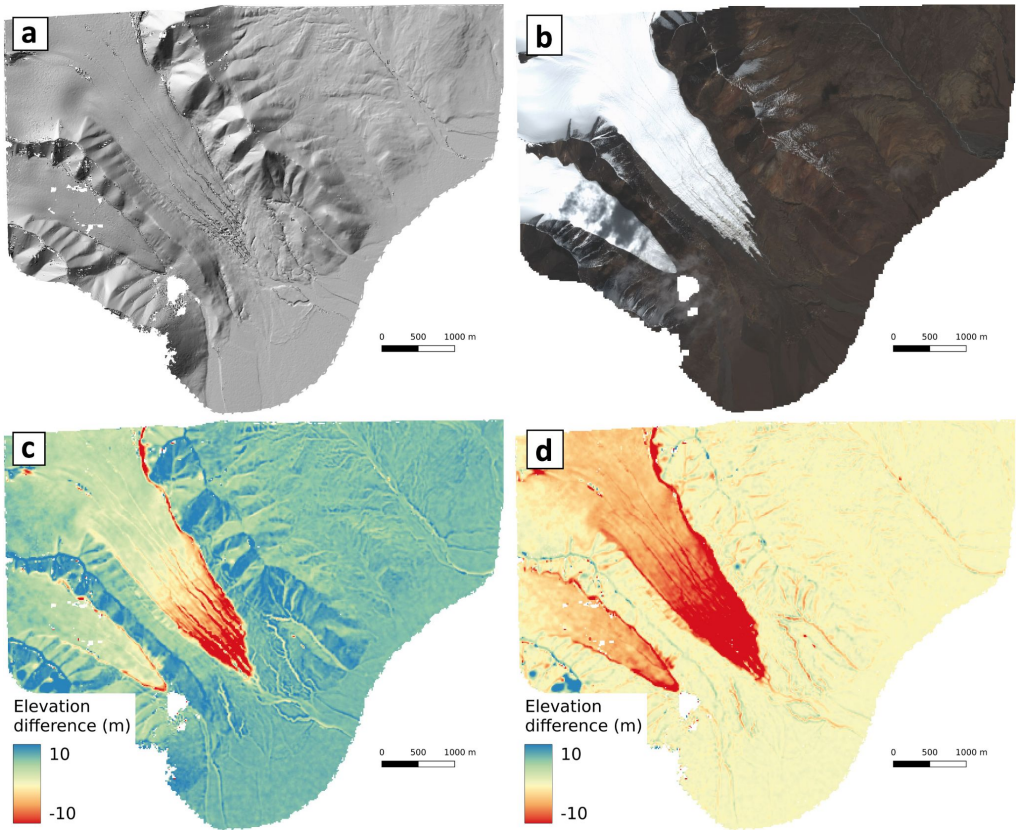

Figure 3. A sample PGO product for the Purogangri ice cap over the Tibetan Plateau (PGO ID: 2018-10-03_0458515_Purogangri_ASC). (a) Shaded relief image of the BM DEM; (b) multi-spectral 2-m ortho-image; (c) Elevation difference of the Pléiades DEMs with the Copernicus 30 DEM prior (c) and after (d) coregistration. For this specific case, the shift vector of the PGO DEMs to GLO-30 were: dEast = −1.8 m ; dNorth = 4.8 m ; dZ = −6.6 m.

7

https://doi.org/10.5194/egusphere-2024-250
Preprint. Discussion started: 21 February 2024

2.3.2. Maps of elevation changes

Once a PGO site is observed again, we generate DEMs from the most recent Pléiades imagery and compare these to the older DEMs to map five (sometimes six or more) years of glacier elevation change (Figure 4). This is achieved in two steps: first the most recent Pléiades DEM is coregistered to the older one on the stable terrain, using the implementation by D. Shean of the Nuth and Kääb (2011)'s algorithm. Next, remaining spatially-coherent elevation biases are corrected by fitting a fifth order polynomial in the across-track direction (Gardelle et al., 2013) and a spline fit along-track (Falaschi et al., 2023). The latter is needed to correct low-frequency undulating biases due to the jitter of the Pléiades satellite platform at a frequency of about 1 Hz (Deschamps-Berger et al., 2020). These along-track biases are not systematic and have a typical amplitude of 1–2 m and a wavelength of about 4 km.

The jitter is especially strong for Pléiades 1B since the year 2021 due to an issue with the satellite platform. These across-track and along-track corrections are only efficient if there is a sufficient amount of well-distributed stable terrain around the glaciers. In the case of the Tuyuksu site (Figure 4), successive corrections allow reducing the dispersion of the residuals by almost a factor of two, e.g. the normalized median absolute deviation (NMAD) is lowered from 2.8 to 1.5 m. The along-track undulations are not entirely removed (Figure 4c), however. Thus, we invite the users to carefully check the stable terrain as an indicator of the quality of the corrections (see also Figure A3 in Berthier et al., in press).

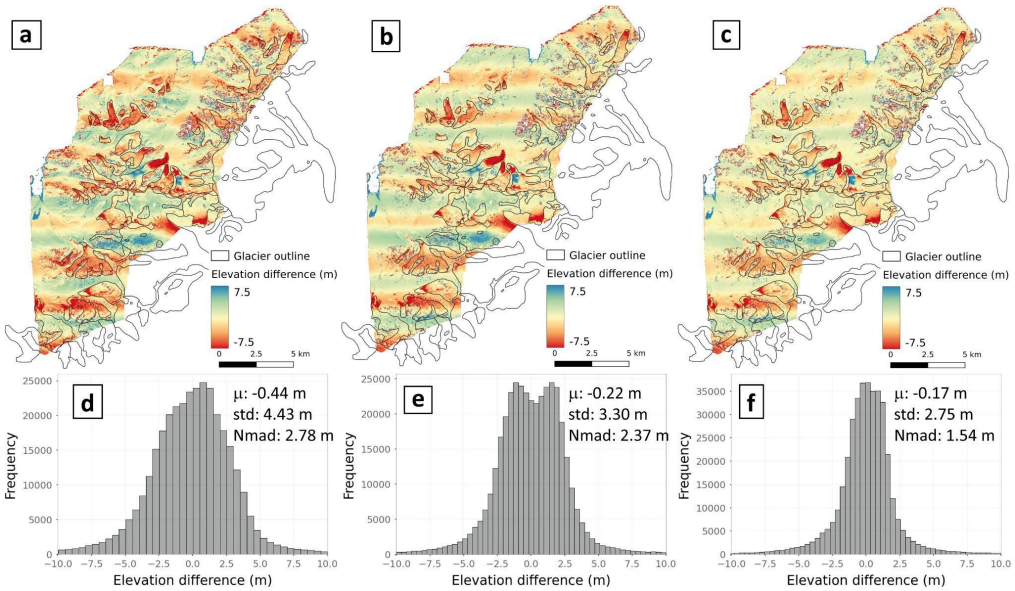

Figure 4. Processing steps to generate the PGO elevation change maps on the Tuyuksu (Central Asia) site in Kazakhstan. The upper panels (a, b, c) show the elevation differences maps from 2016 to 2021 and the lower panels (d, e, f) the distribution of the elevation differences off glaciers. Maps and histograms are shown before coregistration (a, d), after coregistration (b, e) and after bias corrections (c, f). (PGO ID: 2016-08-27_0545099_Tuyuksu_ASC ; 2021-08-21_0546043_Tuyuksu_ASC).

Two, three (and sometimes more) stereo pairs are often needed to cover entirely a single PGO site. After five years, we thus generate the elevation change maps for all possible pairs of overlapping DEMs, at 2

8

https://doi.org/10.5194/egusphere-2024-250
Preprint. Discussion started: 21 February 2024

and 20 m ground sampling distance and for the two algorithms (SGM and BM, Fig. 2). Hence, numerous elevation change maps are computed and we leave it to the users to decide which combination works best for their needs. Basic statistics are provided for each elevation change map (e.g., standard deviation and NMAD off glacier) to guide the users in their choice.

3. Evaluation of the PGO datasets

3.1. Evaluation of the DEMs

3.1.1 Quality of the coregistration to GLO-30

We assess the quality of the coregistration of 259 PGO DEMs to GLO-30 (Figure 5). The spread of the residuals are similar in both easting and northing directions with standard deviations of 5 to 6 m, and the standard deviation is slightly larger than 7 m in the vertical direction. The median shift is almost 0 m in easting direction, whereas the PGO DEMs are slightly shifted (4.5 m) toward the North compared to GLO-30. We have no explanation for this small systematic northward shift. PGO DEMs are, on average, 2.4 m lower than GLO-30. This vertical shift could be due to winter snow affecting the GLO-30 (derived from individual Tandem-X DEMs acquired year round) but not affecting the PGO DEMs, acquired only in summer. We note that these values (mean/standard deviation) do not represent the absolute geolocation performance of the Pléiades DEMs as they are also influenced by any mis-registration of GLO-30 itself.

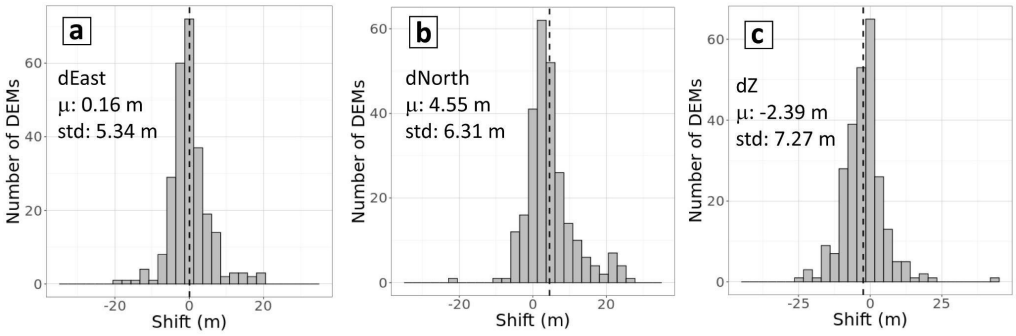

Figure 5. Distributions of the shifts in the easting (a), northing (b) and vertical (c) directions between 265 PGO DEMs acquired between 2016 and 2022 (10 first campaigns) and GLO-30. "μ" stands for the mean, "std" for the standard deviation. The figure only shows the histograms for the BM DEMs. For the semi-global matching DEMs (not shown), the mean and standard deviation of the shifts are almost unchanged, within a few tenth of centimetres.

Coregistration to GLO-30 failed or led to unreliable horizontal shifts (> 30 m) for about 10% of the sites. Examples of problematic sites include Livingstone Island (Subantarctic and Antarctic Islands) where GLO-30 displays large artefacts, possibly due to errors during the unwrapping of the TanDEM-X interferograms. Hence for seven DEMs out of nine on this Island, we applied no coregistration. Coregistration also failed in a few cases where very limited stable terrain was available (e.g., on Balleny Islands around Antarctica). When coregistration failed or was judged unreliable, the Pléiades DEM were

9

https://doi.org/10.5194/egusphere-2024-250
Preprint. Discussion started: 21 February 2024

left unchanged (i.e. not shifted) and the unsuccessful coregistration was identified on the metadata sheet accompanying each PGO product.

3.1.2 Comparison of close-in-time PGO DEMs in their overlapping areas

As several Pléiades DEMs are sometimes needed to cover a PGO site, they include overlapping areas where the DEMs acquired a few days/weeks apart can be compared. These overlapping areas provide an opportunity to assess the performance of the coregistration, the so-called "triangulation" in Nuth and Kääb (2011). Indeed, after coregistration to GLO-30, we expect two overlapping Pléiades DEMs to be well-coregistered, and residual shifts between the DEMs can be interpreted as coregistration errors (Figure 6).

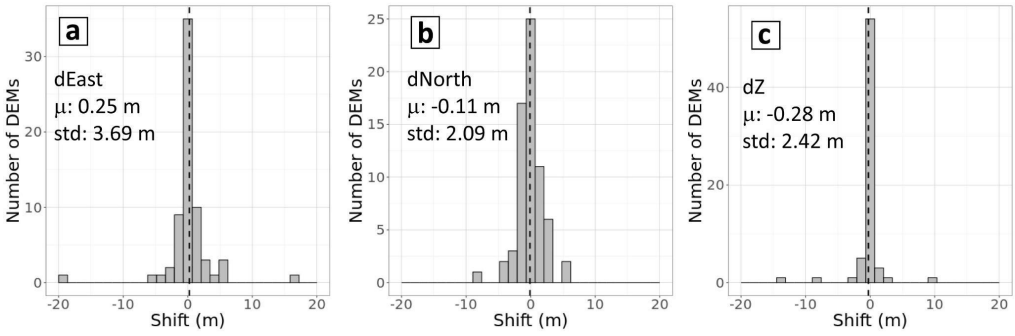

Figure 6. Same as figure 5 but for the shifts between the PGO DEMs over their overlapping portion (n=64). We only show the results for the 2 m BM DEMs. Results are very similar for the semi-global matching DEMs and at both resolutions (2 m and 20 m).

The mean residuals are very close to 0 m in all directions and the standard deviations range from 2 to 4 m. This reflects the quality of the coregistration to GLO-30. We note that a few PGO DEMs show residual shifts of over 10 m. They correspond to sites in areas of high relief (e.g., glacier Fedchenko in Tadjikistan or Makalu in Nepal) where GLO-30 is subjected to large errors.

3.1.3 Evaluation of the PGO DEMs using simultaneous lidar data

In Norway and western Canada, airborne lidar campaigns fortuitously acquired data with a separation time of one day or less of Pléiades stereo collection (Table 2). This ideal situation allows us to evaluate the performance of the PGO DEMs because of negligible glacier elevation change. Hence, the elevation difference directly reflects the uncertainties of the PGO DEMs. Uncertainties based on repeated lidar acquisitions over stable terrain typically yield errors (~0.1 m) that are almost one order of magnitude smaller than those of the PGO DEMs, hence they are neglected here. The simultaneity of the surveys allows comparison of the uncertainties of the PGO DEMs on and off glacier, an important aspect as, in general, one has to assume that the off glacier terrain is representative of the glacier terrain (Hugonnet et al., 2022). For this comparison, we use the final PGO DEMs, coregistered to GLO-30.

The lidar pointclouds were triangulated and linearly interpolated into 1 m gridded DEMs using ASP. For the comparison, we coregistered each PGO DEM (i.e., BM and SGM) with each synchronous lidar (Shean et al., 2016; Nuth and Kääb, 2011). The DEM coregistration was done using the RGI v6.0 (RGI Consortium, 2017) glacier inventory as a mask to define the stable terrain, and in this process the lidar

10

https://doi.org/10.5194/egusphere-2024-250
Preprint. Discussion started: 21 February 2024

DEMs were bilinearly re-sampled to 2x2 m in order to match the resolution of the Pléiades DEMs.

To evaluate the quality of the PGO DEMs, we calculated different statistics to characterise DEM uncertainties, based on the maps of elevation difference between Pléiades and lidar (Fig. 7): NMAD off-glacier and on-glacier, median off-glacier and on-glacier (Table 3). For these statistics, on- and off- glacier terrain was classified using high resolution glacier outlines manually digitized on the Pléiades orthoimages and a hillshade representation of the lidar DEMs.

Table 2. Characteristics of the lidar surveys used to evaluate the PGO DEMs.

Region	Surveyed glaciers	Glacier area (km²)	Date PGO/lidar YYYY-MM-DD	PGO /Geostore ID	Lidar p/m²	Avg Slope on/off glacier
Western Canada	Peyto	47.0	2016-09-13 / 2016-09-13	2016-09-13_1912075_Wapta_WNA / DS_PHR1B_201609131912075_FR1_PX_W117N51_0616_02636	1	13°/28°
North Norway	Langfjordjøkelen	6.4	2018-09-01 / 2018-09-01	NaN / DS_PHR1B_201809011030275_FR1_PX_E021N70_0604_01124*	2	12°/31°
South Norway	Hellstugubreen, Gråsubreen, Vestre Memurubreen, Austre Memurubreen	19.7	2019-08-27 / 2019-08-26	2019-08-27_1102544_Jotunheinmen_SCA / DS_PHR1B_201908271102544_FR1_PX_E008N61_0615_01712	2	11°/26°

*Langfjordjøkelen was surveyed by the PGO one year earlier, 8 September 2017. This 2018 Pléiades stereo pair was not acquired as part of the PGO, this is why we only provide the ID of the Pléiades stereo pair in the Geostore Airbus D&S catalogue.

11

https://doi.org/10.5194/egusphere-2024-250
Preprint. Discussion started: 21 February 2024

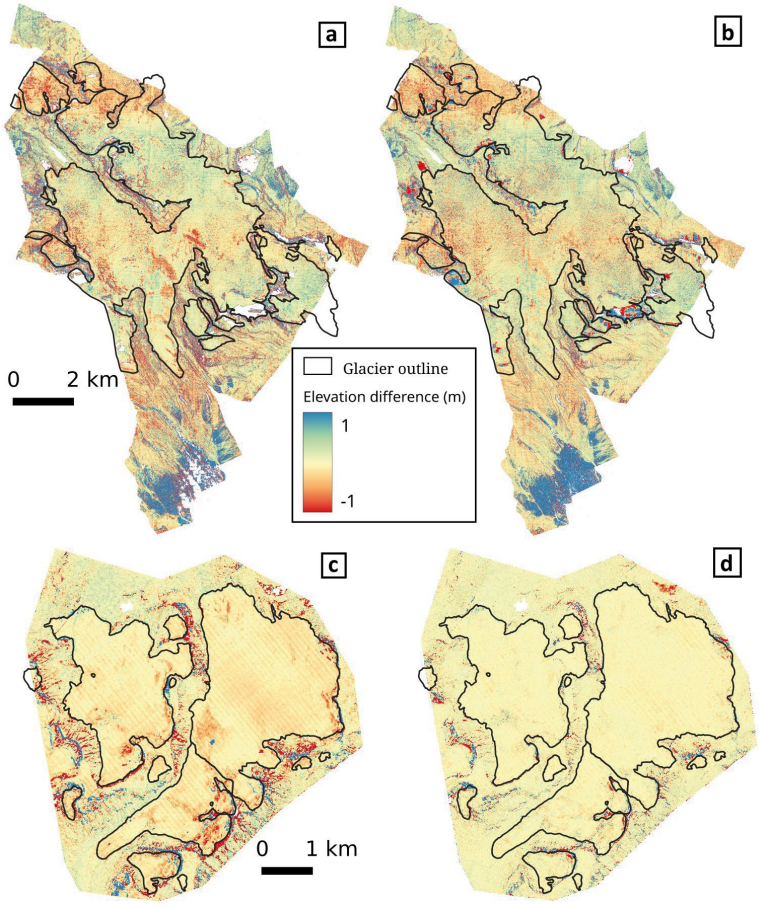

Figure 7. Map of elevation differences between PGO and Lidar DEMs acquired the same day over Peyto Glacier (13 September 2016, Canada, panels a and b) and one day apart over Hellstugubreen (26 and 27 August 2019, Norway, panels c and d). We do not show here the map of elevation difference for other glaciers in Norway (Langfjordjøkelen, Gråsubreen) because the patterns are highly similar. BM - Block matching. SGM - Semi-global matching.

12

https://doi.org/10.5194/egusphere-2024-250
Preprint. Discussion started: 21 February 2024

Table 3. Statistics on the elevation differences (m) between the PGO DEMs and the Lidar DEMs acquired the same day. BM - Block matching. SGM - Semi-global matching. "Hellstugubreen" stands for "Hellstugubreen, Gråsubreen, Vestre Memurubreen, Austre Memurubreen".

	Median Dh off glac (m)	Median Dh on glac (m)	NMAD off glac (m)	NMAD on glac (m)
2016 Peyto - BM	0.02	−0.01	0.59	0.36
2016 Peyto - SGM	0.03	0.00	0.46	0.41
2018 Langfjordjøkelen - BM	0.01	−0.19	0.67	0.14
2018 Langfjordjøkelen - SGM	0.01	−0.14	0.54	0.17
2019 Hellstugubreen - BM	−0.01	−0.12	0.38	0.12
2019 Hellstugubreen - SGM	0.00	−0.09	0.29	0.15

By construction, the median elevation differences off glaciers are very close to 0 m. Over glacierized terrain, biases are also modest. Almost null for Peyto Glacier, they are slightly negative for the Norwegian sites but always within 0.2 m. Conversely, the dispersion of the residuals are slightly larger for the Canadian site, with a NMAD of about 0.4 m, while it ranges between 0.12 and 0.21 m for the glaciers in Norway. We note that the NMAD are systematically larger off glaciers than on glaciers which confirms that using the off glacier terrain to infer the uncertainty on glaciers is a conservative approach. Interestingly the choice of the correlation algorithm (BM or SGM) has a different influence on and off glaciers. SGM is superior off glaciers whereas using BM leads to reduced NMAD on glaciers.

The median elevation difference and its spread (quantified using the NMAD) are rather constant with elevation (Figure 7, only shown for the Peyto site, Canada). Off glacier, the positive elevation differences at low elevations are explained by the presence of vegetation (see also the southernmost portion of the map in Figure 7a-b). The Pléiades summer DEMs map the height of the canopy while the lidar maps the bare ground below the vegetation (Piermattei et al., 2019). The bias and the NMAD are constant up to slopes of 50°. Above, the dispersion of the elevation difference increases rapidly (on and off glacier) and the median difference departs from 0. These results indicate that a good practice is to exclude areas of high reliefs (e.g., slopes larger than 50°) when computing the glacier-wide mean elevation changes.

13

https://doi.org/10.5194/egusphere-2024-250
Preprint. Discussion started: 21 February 2024

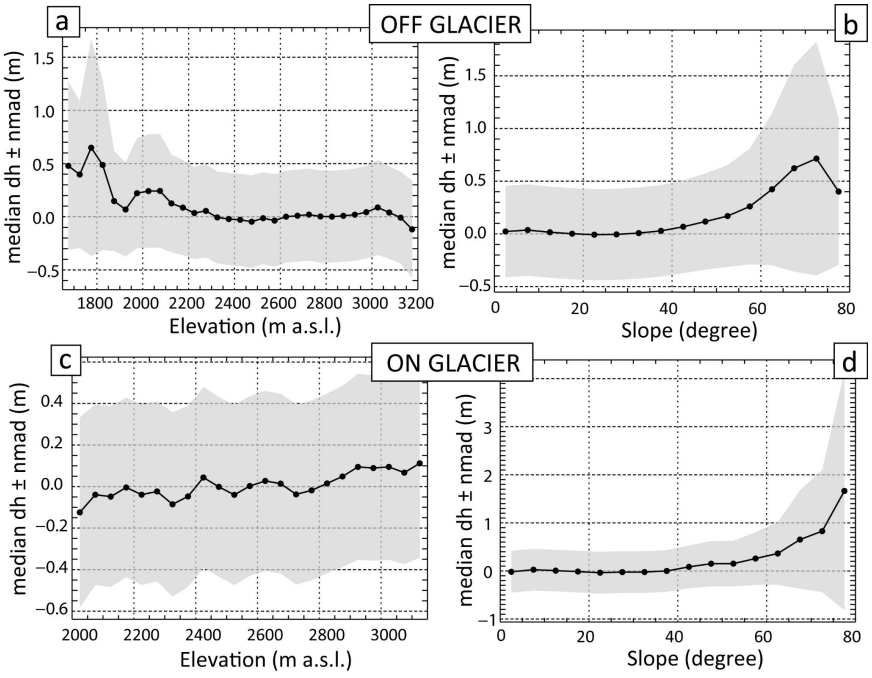

Figure 8. Median elevation differences (dh) between the Pléiades SGM DEMs and the lidar DEMs for the Peyto Glacier site (Canada). Median dh are plotted with elevation (left panels) and slope (right panels) off glaciers (upper panels) and on glaciers (lower panels). The grey shading corresponds to ± one NMAD about the median.

Overall, these evaluations using lidar data suggest that glacier elevation changes can be measured from Pléiades DEMs with a decimetric accuracy, with a minor influence of the processing algorithm. We note that these evaluations are performed on relatively small glaciers with abundant nearby stable terrain which likely facilitate the coregistration and the bias corrections. So these results may not be readily transferable to larger glaciers.

3.2. Uncertainty of the elevation changes

Uncertainties in the elevation difference from repeat Pléiades DEMs have previously been quantified with centimetric GNSS measurement. In the Mont Blanc massif, such measurements are repeated each year in early September along four transverse profiles on the Mer de Glace and on Argentière glaciers. For the 2021–22 mass balance year, the mean bias of the elevation difference was lower than 0.3 m and its standard deviation lower than 0.4 m (Berthier et al., in press). Similar values were found for elevation difference of Mera Glacier in Nepal from 2012 to 2018, with a mean bias of −0.24 m and standard deviation of 0.52 m (Wagnon et al., 2021).

Here, we quantified the uncertainty of the elevation changes systematically, taking advantage of the depth of the PGO archive. We used the elevation difference off glacier (as mapped in RGI v6.0) as a proxy of the uncertainty on glaciers. This is a conservative choice as the errors of the DEMs tend to increase with slope (Toutin, 2002; Lacroix, 2016; Hugonnet et al., 2022) and the average slopes are often gentler on glaciers than on nearby ice-free terrain (see also section 3.1.3). This is also conservative because during the five year time span separating the PGO DEMs, the off glacier terrain has evolved due to e.g., vegetation changes, destabilisation of recently deglaciated slopes. We calculated uncertainties

14

https://doi.org/10.5194/egusphere-2024-250
Preprint. Discussion started: 21 February 2024

(at the 95% confidence level) on the mean elevation change over a given area (ranging from 0.01 km² to 10 km²) using the patch method (Miles et al., 2018; Dussaillant et al., 2018). For a given patch size, we extract the 95th percentile of the absolute mean elevation difference. We analysed 58 PGO elevation difference maps for which the off glacier terrain covered at least 50 km² (Figure 9).

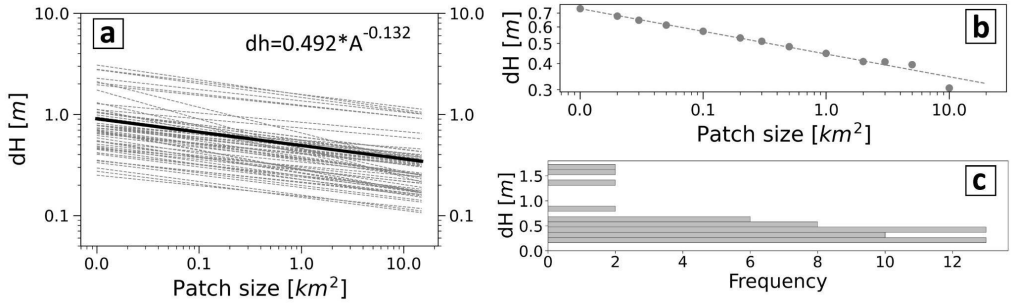

Figure 9. (a) Uncertainties (dh) at the 95% confidence level (2-sigma) for 58 PGO maps of elevation changes as a function of the averaging area. The dashed lines correspond to individual maps of elevation changes obtained from the 2-m BM DEMs and for which the stable terrain occupies more than 50 km². The thick black line corresponds to the mean of all these individual lines and its equation is provided. (b) Example of the uncertainty (at the 95% confidence interval) as a function of the patch size for one of the PGO repeat surveys on Langfjordjokelen in Norway. (c) Distribution of the uncertainties for the 58 elevation difference maps and a patch size of 1 km².

We observe a relatively large spread of the uncertainties on the elevation differences despite the fact that they are all derived from repeat Pléiades DEMs. For example, the 2-sigma uncertainties for a 1 km² patch size range from 0.15 m up to 1.5 m. The largest uncertainties (between 1.2 and 1.5 m, n=6) correspond to maps of elevation difference affected by a larger jitter in the Pléiades DEMs and only partly corrected by our along-track spline correction. This is for example the case for the Tuyuksu (Central Asia) 2016–2021 elevation difference maps shown in Figure 4. Excluding these peculiar six maps, the remaining uncertainties (95% confidence level) are on average 0.38 m for a 1 km² patch size with a limited spread (n=52, min=0.15, max=0.83, standard deviation = 0.15 m). The variance of the mean slope off glacier only explains a small fraction (13%) of the variance in these uncertainties. These mean uncertainties are in agreement with the one derived from same-day lidar surveys (section 3.1.3).

4. Are PGO sites representative of the Earth's glaciers?

The ASTER sensor, on board the TERRA platform, is the only satellite mission in orbit providing publicly-available global coverage using optical stereoscopic images. Recently, it was used to generate maps of elevation changes and hence to calculate glacier-wide mass balances for almost all the Earth's glaciers from 2000 to 2019 (Hugonnet et al., 2021). However, ASTER will stop acquiring images in 2025 (or 2026) and no satellite mission is scheduled to provide publicly-available, global coverage with stereo images. Very high resolution sensors like Pléiades do not have the capability to replace ASTER. It is useful, however, to assess whether the 140 glacier sites surveyed by the PGO provide a reasonable assessment of glacier mass change for Earth's glaciated environments.

15

https://doi.org/10.5194/egusphere-2024-250
Preprint. Discussion started: 21 February 2024

To determine the representativeness of the PGO sampling, we extracted from the Hugonnet et al. database, the glacier-wide mass balance of glaciers intersecting the PGO sites (named hereafter 'PGO glaciers'). For glaciers only partly covered in a PGO site, we retained those with at least 50% coverage. There are about 6800 PGO glaciers and, in area, they cover 2.5% of the world's glaciers (Table 3). By region, the coverage is highly heterogeneous and varies from 0% in the Russian Arctic to almost 47% in New Zealand.

For each GTN-G first order glacier region, we then computed the region-wide mass balances as the area-weighted sum of the PGO glacier-wide mass balances and compared these regionally-aggregated values to the Hugonnet et al.'s values, using the full sample of glaciers. Three periods were considered, 2000–2019, i.e. the full period for which the uncertainties are the smallest in Hugonnet et al. database and also two sub-periods, 2000–09 and 2010–19, to test the ability of PGO glaciers to capture the change in mass balance from one decade to another (Figure 10).

At global scale, excluding the unsampled Russian Arctic, the global mass balance during 2000–19 was −0.39±0.02 w.e./yr (Hugonnet et al., 2021). Using only the values for PGO glaciers (Table 4), the global mass balance is slightly more negative (−0.46 m w.e./yr). PGO glaciers capture rather well the acceleration of the mass loss that occurred from 2000–09 to 2010–19. The full sample indicates a drop of the mass balance by 0.05 m w.e./yr between the two periods, PGO glaciers see an almost identical drop of 0.07 m w.e./yr.

At the scale of the 18 individual GTN-G first order regions (Figure 10, Table 4, Russian Arctic excluded), the mass balance differences between the full sample and PGO glaciers are larger. When the 20-yr period is considered, the differences in region-wide mass balance can be as large as 0.34 m w.e./yr (region: Iceland) with a standard deviation of 0.16 m w.e./yr (n=18). Again, PGO glaciers perform better at capturing the change in mass balance between the two 10-yr periods: the maximum difference is 0.21 m w.e./yr (region: Western Canada and USA) and the minimum difference is −0.15 m w.e./yr (regions: South Asia West and Subantarctic and Antarctic Islands), the standard deviation being 0.09 m w.e./yr. For 10 out of 18 RGI regions, the change in region-wide mass balance is observed by PGO glaciers with an error of less than 0.05 m w.e./yr.

Hence, even if the PGO sites were not chosen to represent the World's glaciers, they still provide a reasonable estimate of their mass balance and perform even better at capturing their temporal changes. Yet, one strong complication to use these glaciers for a global mass change analysis would be related to the fact that the Pléiades acquisitions on the 140 PGO glacier sites are not performed simultaneously but using a moving temporal window (Table 1).

It should be noted that there are uncertainties in the Hugonnet et al (2021) data and that they are not necessarily representative for smaller samples of glaciers or shorter periods (e.g., Andreassen et al., 2023; Berthier et al., 2023). At local scale and for periods of a few months or years, repeated lidar or other high resolution DEMs (e.g. PGO) give more accurate results.

16

https://doi.org/10.5194/egusphere-2024-250
Preprint. Discussion started: 21 February 2024

Table 3. Fraction of the Earth's glacier sampled by the PGO. The number and area of glaciers refer to the RGI v6.0 inventory except in region 12 (Caucasus and Middle East) where the Global Land Ice Measurements from Space (GLIMS) outlines are used, as in Hugonnet et al. 2021.

	GTN-G region	Number of glaciers	Glacier area km²	Number of PGO sites	Number of PGO glaciers*	Area of PGO glaciers (in % of the total)
1	Alaska	27,108	86,725	6	190	1.0
2	Western Canada and USA	18,855	14,524	5	268	3.5
3	Arctic Canada North	4556	105,111	4	22	0.4
4	Arctic Canada South	7415	40,888	2	54	0.8
5	Greenland Periphery	19,306	89,717	8	255	1.9
6	Iceland	568	11060	1	17	1.6
7	Svalbard and Jan Mayen	1615	34187	6	60	3.2
8	Scandinavia	3417	2949	5	238	17.3
9	Russian Arctic	1069	51,592	0	0	0
10	North Asia	5151	2410	2	113	7.1
11	Central Europe	3927	2092	13	882	33.3
12	Caucasus and Middle East	3516	1336	3	344	25.8
13	Central Asia	54,429	49,303	12	1185	4.5
14	South Asia West	27,988	33,568	5	301	1.7
15	South Asia East	13,119	14,734	9	624	7.9
16	Low Latitudes	2939	2341	9	220	12.6
17	Southern Andes	15,908	29,429	30	894	10.3
18	New Zealand	3537	1162	6	935	46.8
19	Subantarctic and Antarctic Islands	2752	132,867	14	208	2.2
	Global	**217,715**	**705,995**	**140**	**6810**	**2.5**
	Global excl. Russian Arctic	**216,106**	**654,405**	**140**	**6810**	**2.7**

* We only count glaciers for which at least 50% of the area is covered.

17

https://doi.org/10.5194/egusphere-2024-250
Preprint. Discussion started: 21 February 2024

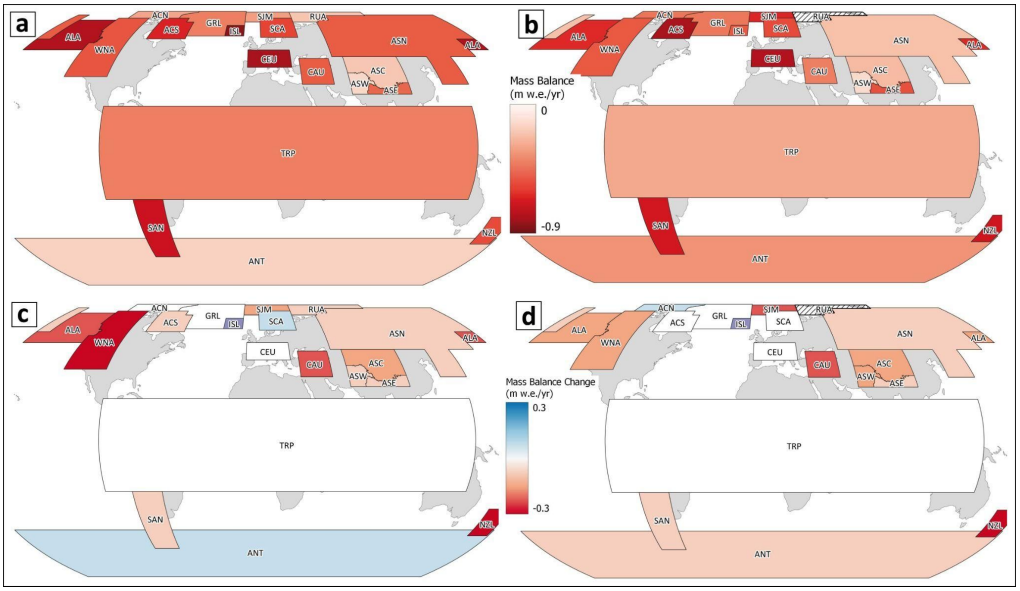

Figure 10. Comparison of the 2000-2019 region-wide mass balances calculated using the entire Hugonnet et al. (2021)'s dataset (a) and using only the glaciers sampled by the PGO (b). The lower panels show the changes in region-wide mass balances between 2000-2009 and 2010-2019 for (c) all glaciers and for (d) the subset of glaciers sampled by the PGO.

18

https://doi.org/10.5194/egusphere-2024-250
Preprint. Discussion started: 21 February 2024

Table 4. Regional and global mass balances (in m w.e./yr) from the entire RGI sample (Hugonnet et al., 2021) and from the PGO glaciers (this study). MB stands for mass balance. Delta_MB corresponds to the change in region-wide mass balance from 2000–09 to 2010–19.

	GTN-G region	MB 2000-19 ALL	MB 2000-19 PGO	Delta_MB ALL	Delta_MB PGO
1	Alaska	−0.77	−0.63	0.12	0.16
2	Western Canada and USA	−0.52	−0.51	−0.10	0.11
3	Arctic Canada North	−0.29	−0.43	-0.18	−0.09
4	Arctic Canada South	−0.65	−0.79	−0.21	−0.06
5	Greenland Periphery	−0.40	−0.42	0.00	−0.04
6	Iceland	−0.85	−0.51	0.36	0.32
7	Svalbard and Jan Mayen	−0.31	−0.64	−0.28	−0.39
8	Scandinavia	−0.57	−0.55	0.05	−0.01
9	Russian Arctic	−0.20	NaN	−0.06	NaN
10	North Asia	−0.50	−0.21	0.28	0.31
11	Central Europe	−0.80	−0.77	0.05	0.00
12	Caucasus and Middle East	−0.50	−0.40	0.08	0.12
13	Central Asia	−0.19	−0.23	−0.02	−0.05
14	South Asia West	−0.14	−0.13	0.08	−0.07
15	South Asia East	−0.47	−0.53	−0.05	−0.08
16	Low Latitudes	−0.40	−0.28	0.12	0.10
17	Southern Andes	−0.70	−0.68	0.02	0.01
18	New Zealand	−0.55	−0.69	−0.10	−0.18
19	Subantarctic and Antarctic Islands	−0.16	−0.34	−0.10	−0.25
	Global excl. Russian Arctic	**−0.39**	**−0.46**	**−0.05**	**−0.07**

5. Conclusion

The Pléiades Glacier Observatory is an initiative by the French Space Agency (CNES) and LEGOS to facilitate access to very high resolution digital elevation models and, after signing a licence, ortho-images of glaciers. Such data are useful to calculate glacier geodetic mass balances, but also to support other glaciology oriented applications, such as updating glacier outlines, extracting glacier hypsometry or qualitatively documenting glacier changes. The PGO aims at managing the Pléiades acquisitions, and distributing products that are tailored for glaciological applications, and as user friendly as possible. The acquisitions started in 2016 and during the first five years, acquired stereo-pairs over 140 target sites around the globe, selected through a call to the glaciological community. Since 2021, these acquisitions have been progressively repeated to produce maps of elevation change over five years. At the time of writing, already 31 publications used PGO data to examine glacier changes.

We quantified the uncertainties of the DEMs and elevation change maps derived from repeat Pléiades

19

https://doi.org/10.5194/egusphere-2024-250
Preprint. Discussion started: 21 February 2024

DEMs. This was done with two methods: (1) comparison to simultaneous accurate lidar surveys, and (2) using the stable terrain as a proxy of the uncertainties on glaciers. Both methods agree broadly on the uncertainties, and as a rule of thumb, the glacier-wide elevation differences have a 2-sigma uncertainty of about 0.5 m for a glacier of 1 km² or larger. While these uncertainties characterise the area-averaged elevation change between two Pléiades DEM, other sources of error exist for geodetic mass balance such as uncertainties in glacier area and on the volume to mass conversion factor.

Pléiades satellites are planned to orbit until 2026. Access to data from their successors (Pléiades Neo) is not yet secured for the scientific community and the cost may be prohibitive. It should be a priority for the space agencies to continue to provide high resolution stereo-imagery to scientists to observe the imprint of climate change on the Earth surface and in particular on glaciers.

Data availability statement

Pléiades Glacier Observatory DEMs are under CC-BY-NC licence and freely available at: https://a2s-dissemination.u-strasbg.fr/#!

Licensing issues prevent us from openly distributing the Pléiades ortho-images. They are available after signing the Pléiades institutional scientific licence to be requested to the French space agency CNES (dinamis@cnes.fr).

At the time of submission, the elevation change products cannot be accessed yet on a map server. They are available upon request to the corresponding author. As soon as a distribution platform is operational, data availability will be advertised on the PGO website (https://www.legos.omp.eu/pgo/).

The scripts used to generate the DEMs and ortho-images and to coregister them to GLO-30 are available upon request to the corresponding author.

Author contributions

EB designed the PGO program. JL and EB generated the DEMs and elevation change maps. JMCB, LMA and BM provided Lidar data and all related analysis. DF and SH helped with the project design and the image acquisitions. All authors contributed to the discussion of the results. CB worked on the regional representativity of the PGO sites. EB prepared the manuscript with contributions from all co-authors

Competing interests

One author (EB) is a member of the editorial board of The Cryosphere.

Acknowledgments

E. Berthier and J. Lebreton acknowledge support from the French Space Agency (CNES). B. Menounos acknowledges funding from the Natural Sciences and Engineering Research Council of Canada and the Tula Foundation. L.M. Andreassen acknowledges the internal NVE project 'N80524 Regionalt massebalanseestimat av norske breer'. This is also a contribution to the International Association of Cryospheric Sciences (IACS) working group on Regional Assessments of Glacier Mass Change (RAGMAC).

20

https://doi.org/10.5194/egusphere-2024-250
Preprint. Discussion started: 21 February 2024

491 # Appendix

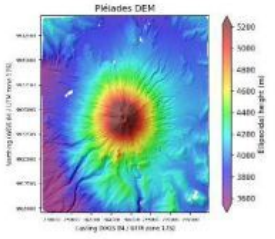

Pléiades Glacier Observatory : DEM

Date : 2016-11-15
Site : Cotopaxi_TRP

DEM information

Coordinate system	UTM 17 south - EPSG 32717
Correlation algorithm	Semi Global Matching (SGM)
DEM resolution	2 m and 20 m
Reference for height	Ellipsoidal Height (WGS84)
Shift vector to Copernicus GLO-30 (m)	dx=-2.69; dy=-2.64; dz=+1.74
Base-to-Height ratio (B/H)	0.42

Source images

PHR DS_PHR1B_201611151534305_FR1_PX_W079S01_0708_01575
PHR DS_PHR1B_201611151535093_FR1_PX_W079S01_0708_01604

Copyright

Pléiades © CNES Year_of_acquisition, Distribution Airbus D&S

Archive structure

```
└2016-11-15_1535065_Cotopaxi_TRP
  ├BM
  ├2016-11-15_1535065_Cotopaxi_TRP_footprint.shp
  ├2016-11-15_1535065_Cotopaxi_TRP_footprint.dbf
  ├2016-11-15_1535065_Cotopaxi_TRP_footprint.prj
  ├2016-11-15_1535065_Cotopaxi_TRP_footprint.shx
  └SGM
    ├2016-11-15_1535065_Cotopaxi_TRP_1B_DEM_SGM_2m.tif
    ├2016-11-15_1535065_Cotopaxi_TRP_1B_DEM_SGM_20m.tif
    ├README_SGM_DEM.pdf
    ├PREVIEW_2016-11-15_1535065_Cotopaxi_TRP_1B_DEM_SGM_20m.png
    └Coreg_2016-11-15_1535065_Cotopaxi_TRP_1B_DEM_SGM_20m_vs_Cop30.png
```

Description

DEMs and orthoimages where generated from raw Pléiades images using the Ames Stereo Pipeline [Beyer et al., 2018]. The set of processing parameters used for DEM generation are from [Marti et al., TC, 2016] for block matching -BM- and from [Deschamps-Berger et al., 2020] for semi global matching -SGM.

All DEMs and orthoimages are coregistered on the Copernicus GLO-30 DEM using the demcoreg tool [Shean et al., 2021].

Acknowledgement statement: The Pléiades images/DEMs used in this study was provided by the Pléiades Glacier Observatory initiative of the French Space Agency (CNES) and Laboratoire d'Etudes en Géophysique et Océanographie Spatiales (LEGOS).

When an image is shown in a presentation, website or an article, the copyright should be (Pléiades © CNES Year_of_acquisition, Distribution Airbus D&S).

We remind to cope with the licence rules regarding (no) data sharing and no commercial use.

References

Beyer et al.: The Ames Stereo Pipeline: NASA's Open Source Software for Deriving and Processing Terrain Data, Earth and Space Science, 5(9), 537–548, doi:10.1029/2018EA000409, 2018.

Shean et al.: dshean/demcoreg, Zenodo, v1.1.0, https://doi.org/10.5281/zenodo.5733347, 2021.

Deschamps-Berger et al.: Snow depth mapping from stereo satellite imagery in mountainous terrain: evaluation using airborne laser-scanning data, The Cryosphere, 14(9),2925–2940, https://doi.org/10.5194/tc-14-2925-2020, 2020.

Marti et al.: Mapping snow depth in open alpine terrain from stereo satellite imagery, The Cryosphere, 10(4), 1361–1380, doi:10.5194/tc-10-1361-2016, 2016.

492

493 **Appendix A1: Example of the fact sheet accompanying each PGO product, here the semi-global matching (SGM)**
494 **DEMs over the Cotopaxi area acquired 15 November 2016.**

21

https://doi.org/10.5194/egusphere-2024-250
Preprint. Discussion started: 21 February 2024

References

Andreassen, L. M., Elvehøy, H., Kjøllmoen, B., and Engeset, R. V.: Reanalysis of long-term series of glaciological and geodetic mass balance for 10 Norwegian glaciers, The Cryosphere, 10, 535–552, https://doi.org/10.5194/tc-10-535-2016, 2016.

Andreassen, L. M., Nagy, T., Kjøllmoen, B., and Leigh, J. R.: An inventory of Norway's glaciers and ice-marginal lakes from 2018–19 Sentinel-2 data, J. Glaciol., 1–22, https://doi.org/10.1017/jog.2022.20, 2022.

Andreassen, L. M., Robson, B. A., Sjursen, K. H., Elvehøy, H., Kjøllmoen, B., and Carrivick, J. L.: Spatio-temporal variability in geometry and geodetic mass balance of Jostedalsbreen ice cap, Norway, Ann. Glaciol., 1–18, https://doi.org/10.1017/aog.2023.70, 2023.

Belart, J. M. C., Berthier, E., Magnússon, E., Anderson, L. S., Pálsson, F., Thorsteinsson, T., Howat, I. M., Aðalgeirsdóttir, G., Jóhannesson, T., and Jarosch, A. H.: Winter mass balance of Drangajökull ice cap (NW Iceland) derived from satellite sub-meter stereo images, The Cryosphere, 11, 1501–1517, https://doi.org/10.5194/tc-11-1501-2017, 2017.

Beraud, L., Cusicanqui, D., Rabatel, A., Brun, F., Vincent, C., and Six, D.: Glacier-wide seasonal and annual geodetic mass balances from Pléiades stereo images: application to the Glacier d'Argentière, French Alps, J. Glaciol., 69, 525–537, https://doi.org/10.1017/jog.2022.79, 2023.

Berthier, E., Vincent, C., Magnússon, E., Gunnlaugsson, Á. Þ., Pitte, P., Le Meur, E., Masiokas, M., Ruiz, L., Pálsson, F., Belart, J. M. C., and Wagnon, P.: Glacier topography and elevation changes derived from Pléiades sub-meter stereo images, The Cryosphere, 8, 2275–2291, https://doi.org/10.5194/tc-8-2275-2014, 2014.

Berthier, E., Floriciou, D., Gardner, A. S., Gourmelen, N., Jakob, L., Paul, F., Treichler, D., Wouters, B., Belart, J. M. C., Dehecq, A., Dussaillant, I., Hugonnet, R., Kääb, A., Krieger, L., Pálsson, F., and Zemp, M.: Measuring glacier mass changes from space—a review, Rep. Prog. Phys., 86, 036801, https://doi.org/10.1088/1361-6633/acaf8e, 2023.

Berthier, E., Vincent, C., and Six, D.: Exceptional thinning through the entire altitudinal range of Mont-Blanc glaciers during the 2021/22 mass balance year, J. Glaciol., https://doi.org/10.1017/jog.2023.100, in press.

Bhattacharya, A., Bolch, T., Mukherjee, K., King, O., Menounos, B., Kapitsa, V., Neckel, N., Yang, W., and Yao, T.: High Mountain Asian glacier response to climate revealed by multi-temporal satellite observations since the 1960s, Nat. Commun., 12, 4133, https://doi.org/10.1038/s41467-021-24180-y, 2021.

Błaszczyk, M., Ignatiuk, D., Grabiec, M., Kolondra, L., Laska, M., Decaux, L., Jania, J., Berthier, E., Luks, B., Barzycka, B., and Czapla, M.: Quality Assessment and Glaciological Applications of Digital Elevation Models Derived from Space-Borne and Aerial Images over Two Tidewater Glaciers of Southern Spitsbergen, Remote Sens., 11, 1121, https://doi.org/10.3390/rs11091121, 2019.

Brun, F., Buri, P., Miles, E. S., Wagnon, P., Steiner, J., Berthier, E., Ragettli, S., Kraaijenbrink, P., Immerzeel, W. W., and Pellicciotti, F.: Quantifying volume loss from ice cliffs on debris-covered glaciers using high resolution terrestrial and aerial photogrammetry, J. Glaciol., 62, 684–695, https://doi.org/10.1017/jog.2016.54, 2016.

Brun, F., Berthier, E., Wagnon, P., Kääb, A., and Treichler, D.: A spatially resolved estimate of High Mountain Asia glacier mass balances from 2000 to 2016, Nat. Geosci., 10, 668–673, https://doi.org/10.1038/ngeo2999, 2017.

Deschamps-Berger, C., Gascoin, S., Berthier, E., Deems, J., Gutmann, E., Dehecq, A., Shean, D., and Dumont, M.: Snow depth mapping from stereo satellite imagery in mountainous terrain: evaluation using airborne laser-scanning data, The Cryosphere, 14, 2925–2940, https://doi.org/10.5194/tc-14-2925-2020, 2020.

Dussaillant, I., Berthier, E., and Brun, F.: Geodetic Mass Balance of the Northern Patagonian Icefield from 2000 to 2012 Using Two Independent Methods, Front. Earth Sci., 6, 8,

22

https://doi.org/10.5194/egusphere-2024-250
Preprint. Discussion started: 21 February 2024

https://doi.org/10.3389/feart.2018.00008, 2018.
Falaschi, D., Berthier, E., Belart, J. M. C., Bravo, C., Castro, M., Durand, M., and Villalba, R.: Increased mass loss of glaciers in Volcán Domuyo (Argentinian Andes) between 1962 and 2020, revealed by aerial photos and satellite stereo imagery, J. Glaciol., 69, 40–56, https://doi.org/10.1017/jog.2022.43, 2023.
Franks, S. and Rengarajan, R.: Evaluation of Copernicus DEM and Comparison to the DEM Used for Landsat Collection-2 Processing, Remote Sens., 15, https://doi.org/10.3390/rs15102509, 2023.
Gardelle, J., Berthier, E., Arnaud, Y., and Kääb, A.: Region-wide glacier mass balances over the Pamir-Karakoram-Himalaya during 1999–2011, The Cryosphere, 7, 1263–1286, https://doi.org/10.5194/tc-7-1263-2013, 2013.
Gleyzes, M. A., Perret, L., and Kubik, P.: Pléiades system architecture and main performances, Int Arch Photogramm. Remote Sens Spat. Informat Sci, 39, 537–542, 2012.
GTN-G: GTN-G Glacier Regions. Global Terrestrial Network for Glaciers., https://doi.org/10.5904/gtng-glacreg-2023-07, 2023.
Hirschmuller, H.: Stereo Processing by Semiglobal Matching and Mutual Information, IEEE Trans Pattern Anal Mach Intell, 30, 328–341, 2008.
Howat, I. M., Porter, C., Smith, B. E., Noh, M.-J., and Morin, P.: The Reference Elevation Model of Antarctica, The Cryosphere, 13, 665–674, https://doi.org/10.5194/tc-13-665-2019, 2019.
Hugonnet, R., McNabb, R., Berthier, E., Menounos, B., Nuth, C., Girod, L., Farinotti, D., Huss, M., Dussaillant, I., Brun, F., and Kääb, A.: Accelerated global glacier mass loss in the early twenty-first century, Nature, 592, 726–731, https://doi.org/10.1038/s41586-021-03436-z, 2021.
Hugonnet, R., Brun, F., Berthier, E., Dehecq, A., Mannerfelt, E. S., Eckert, N., and Farinotti, D.: Uncertainty analysis of digital elevation models by spatial inference from stable terrain, IEEE J. Sel. Top. Appl. Earth Obs. Remote Sens., 15, 6456–6472, https://doi.org/10.1109/JSTARS.2022.3188922, 2022.
Kääb, A., Jacquemart, M., Gilbert, A., Leinss, S., Girod, L., Huggel, C., Falaschi, D., Ugalde, F., Petrakov, D., Chernomorets, S., Dokukin, M., Paul, F., Gascoin, S., Berthier, E., and Kargel, J. S.: Sudden large-volume detachments of low-angle mountain glaciers – more frequent than thought?, The Cryosphere, 15, 1751–1785, https://doi.org/10.5194/tc-15-1751-2021, 2021.
Lacroix, P.: Landslides triggered by the Gorkha earthquake in the Langtang valley, volumes and initiation processes, Earth Planets Space, 68, 1–10, https://doi.org/10.1186/s40623-016-0423-3, 2016.
Lebègue, L., Greslou, D., Blanchet, G., Lussy, F., Fourest, S., Martin, V., Latry, C., Kubik, P., Delvit, J.-M., Dechoz, C., and Amberg, V.: Pléiades-HR satellites image quality commissioning, Rev. Fr. Photogrammétrie Télédétection, 5–10, https://doi.org/10.52638/rfpt.2015.137, 2015.
Loriaux, T. and Ruiz, L.: Spatio-Temporal Distribution of Supra-Glacial Ponds and Ice Cliffs on Verde Glacier, Chile, Front. Earth Sci., 9, 448, https://doi.org/10.3389/feart.2021.681071, 2021.
Małecki, J.: Recent contrasting behaviour of mountain glaciers across the European High Arctic revealed by ArcticDEM data, The Cryosphere, 16, 2067–2082, https://doi.org/10.5194/tc-16-2067-2022, 2022.
Marti, R., Gascoin, S., Berthier, E., de Pinel, M., Houet, T., and Laffly, D.: Mapping snow depth in open alpine terrain from stereo satellite imagery, The Cryosphere, 10, 1361–1380, https://doi.org/10.5194/tc-10-1361-2016, 2016.
Miles, E. S., Watson, C. S., Brun, F., Berthier, E., Esteves, M., Quincey, D. J., Miles, K. E., Hubbard, B., and Wagnon, P.: Glacial and geomorphic effects of a supraglacial lake drainage and outburst event, Everest region, Nepal Himalaya, The Cryosphere, 12, 3891–3905, https://doi.org/10.5194/tc-12-3891-2018, 2018.
Millan, R., Mouginot, J., Rabatel, A., and Morlighem, M.: Ice velocity and thickness of the world's glaciers, Nat. Geosci., 15, 124–129, https://doi.org/10.1038/s41561-021-00885-z, 2022.
Nuth, C. and Kääb, A.: Co-registration and bias corrections of satellite elevation data sets for quantifying glacier thickness change, The Cryosphere, 5, 271–290, https://doi.org/10.5194/tcd-4-2013-2010, 2011.
Paul, F., Frey, H., and Le Bris, R.: A new glacier inventory for the European Alps from Landsat TM scenes

https://doi.org/10.5194/egusphere-2024-250
Preprint. Discussion started: 21 February 2024

of 2003: Challenges and results, Ann. Glaciol., 52, 144–152, 2011.
Pelto, M. S.: Forecasting temperate alpine glacier survival from accumulation zone observations, Cryosphere, 4, 67–75, 2010.
Pfeffer, W. T., Arendt, A. A., Bliss, A., Bolch, T., Cogley, J. G., Gardner, A. S., Hagen, J.-O., Hock, R., Kaser, G., Kienholz, C., Miles, E. S., Moholdt, G., Moelg, N., Paul, F., Radic, V., Rastner, P., Raup, B. H., Rich, J., Sharp, M. J., Andeassen, L. M., Bajracharya, S., Barrand, N. E., Beedle, M. J., Berthier, E., Bhambri, R., Brown, I., Burgess, D. O., Burgess, E. W., Cawkwell, F., Chinn, T., Copland, L., Cullen, N. J., Davies, B., De Angelis, H., Fountain, A. G., Frey, H., Giffen, B. A., Glasser, N. F., Gurney, S. D., Hagg, W., Hall, D. K., Haritashya, U. K., Hartmann, G., Herreid, S., Howat, I., Jiskoot, H., Khromova, T. E., Klein, A., Kohler, J., Konig, M., Kriegel, D., Kutuzov, S., Lavrentiev, I., Le Bris, R., Li, X., Manley, W. F., Mayer, C., Menounos, B., Mercer, A., Mool, P., Negrete, A., Nosenko, G., Nuth, C., Osmonov, A., Pettersson, R., Racoviteanu, A., Ranzi, R., Sarikaya, M. A., Schneider, C., Sigurdsson, O., Sirguey, P., Stokes, C. R., Wheate, R., Wolken, G. J., Wu, L. Z., and Wyatt, F. R.: The Randolph Glacier Inventory: a globally complete inventory of glaciers, J. Glaciol., 60, 537–552, https://doi.org/10.3189/2014JoG13J176, 2014.
Piermattei, L., Marty, M., Ginzler, C., Pöchtrager, M., Karel, W., Ressl, C., Pfeifer, N., and Hollaus, M.: Pléiades satellite images for deriving forest metrics in the Alpine region, Int. J. Appl. Earth Obs. Geoinformation, 80, 240–256, https://doi.org/10.1016/j.jag.2019.04.008, 2019.
Pope, A., Rees, W. G., Fox, A. J., and Fleming, A.: Open Access Data in Polar and Cryospheric Remote Sensing, Remote Sens., 6, 6183–6220, https://doi.org/10.3390/rs6076183, 2014.
Porter, C., Morin, P., Howat, I., Noh, M.-J., Bates, B., Peterman, K., Keesey, S., Schlenk, M., Gardiner, J., Tomko, K., Willis, M., Kelleher, C., Cloutier, M., Husby, E., Foga, S., Nakamura, H., Platson, M., Wethington, M., Jr., Williamson, C., Bauer, G., Enos, J., Arnold, G., Kramer, W., Becker, P., Doshi, A., D'Souza, C., Cummens, P., Laurier, F., and Bojesen, M.: ArcticDEM, , https://doi.org/10.7910/DVN/OHHUKH, 2018.
Rabatel, A., Letréguilly, A., Dedieu, J.-P., and Eckert, N.: Changes in glacier equilibrium-line altitude in the western Alps from 1984 to 2010: evaluation by remote sensing and modeling of the morpho-topographic and climate controls, The Cryosphere, 7, 1455–1471, https://doi.org/10.5194/tc-7-1455-2013, 2013.
RGI 7.0 Consortium: Randolph Glacier Inventory - A Dataset of Global Glacier Outlines, Version 7.0., 2023.
Rounce, D. R., Hock, R., Maussion, F., Hugonnet, R., Kochtitzky, W., Huss, M., Berthier, E., Brinkerhoff, D., Compagno, L., Copland, L., Farinotti, D., Menounos, B., and McNabb, R. W.: Global glacier change in the 21st century: Every increase in temperature matters, Science, 379, 78–83, https://doi.org/10.1126/science.abo1324, 2023.
Sato, Y., Fujita, K., Inoue, H., Sunako, S., Sakai, A., Tsushima, A., Podolskiy, E. A., Kayastha, R., and Kayastha, R. B.: Ice Cliff Dynamics of Debris-Covered Trakarding Glacier in the Rolwaling Region, Nepal Himalaya, Front. Earth Sci., 9, https://doi.org/10.3389/feart.2021.623623, 2021.
Shean, D. E., Alexandrov, O., Moratto, Z. M., Smith, B. E., Joughin, I. R., Porter, C., and Morin, P.: An automated, open-source pipeline for mass production of digital elevation models (DEMs) from very-high-resolution commercial stereo satellite imagery, ISPRS J. Photogramm. Remote Sens., 116, 101–117, https://doi.org/10.1016/j.isprsjprs.2016.03.012, 2016.
Shean, D. E., Bhushan, S., Montesano, P., Rounce, D. R., Arendt, A., and Osmanoglu, B.: A Systematic, Regional Assessment of High Mountain Asia Glacier Mass Balance, Front. Earth Sci., 7, 363, https://doi.org/10.3389/feart.2019.00363, 2020.
Shugar, D. H., Jacquemart, M., Shean, D., Bhushan, S., Upadhyay, K., Sattar, A., Schwanghart, W., McBride, S., de Vries, M. V. W., Mergili, M., Emmer, A., Deschamps-Berger, C., McDonnell, M., Bhambri, R., Allen, S., Berthier, E., Carrivick, J. L., Clague, J. J., Dokukin, M., Dunning, S. A., Frey, H., Gascoin, S., Haritashya, U. K., Huggel, C., Kääb, A., Kargel, J. S., Kavanaugh, J. L., Lacroix, P., Petley, D., Rupper, S., Azam, M. F., Cook, S. J., Dimri, A. P., Eriksson, M., Farinotti, D., Fiddes, J., Gnyawali, K. R., Harrison, S., Jha, M., Koppes, M., Kumar, A., Leinss, S., Majeed, U., Mal, S., Muhuri, A., Noetzli, J., Paul, F., Rashid, I., Sain, K., Steiner, J., Ugalde, F., Watson, C. S., and Westoby, M. J.: A

24

https://doi.org/10.5194/egusphere-2024-250
Preprint. Discussion started: 21 February 2024

massive rock and ice avalanche caused the 2021 disaster at Chamoli, Indian Himalaya, Science, 373, 300, https://doi.org/10.1126/science.abh4455, 2021.

Toutin, T.: Three-dimensional topographic mapping with ASTER stereo data in rugged topography, IEEE Trans. Geosci. Remote Sens., 40, 2241–2247, https://doi.org/10.1109/TGRS.2002.802878, 2002.

Wagnon, P., Brun, F., Khadka, A., Berthier, E., Shrestha, D., Vincent, C., Arnaud, Y., Six, D., Dehecq, A., Ménégoz, M., and Jomelli, V.: Reanalysing the 2007–19 glaciological mass-balance series of Mera Glacier, Nepal, Central Himalaya, using geodetic mass balance, J. Glaciol., 67, 117–125, https://doi.org/10.1017/jog.2020.88, 2021.

Willis, M. J., Herried, B. G., Bevis, M. G., and Bell, R. E.: Recharge of a subglacial lake by surface meltwater in northeast Greenland, Nature, 518, 223–227, 2015.

Zemp, M., Thibert, E., Huss, M., Stumm, D., Rolstad Denby, C., Nuth, C., Nussbaumer, S. U., Moholdt, G., Mercer, A., Mayer, C., Joerg, P. C., Jansson, P., Hynek, B., Fischer, A., Escher-Vetter, H., Elvehøy, H., and Andreassen, L. M.: Reanalysing glacier mass balance measurement series, The Cryosphere, 7, 1227–1245, https://doi.org/10.5194/tc-7-1227-2013, 2013.

25